Ionic liquid route for the corrosion inhibition of Al alloys: the effect of butylammonium nitrate on the corrosion of AA2024-T6

Abdelmoheiman Zakaria Benbouzid, Oumaïma Gharbi, Najet Sidi-Yakoub, Mai T.T. Tran, Mireille Turmine, Vincent Vivier

Research article

Ionic liquid route for the corrosion inhibition of Al alloys: the effect of butylammonium nitrate on the corrosion of AA2024-T6

Abdelmoheiman Zakaria Benbouzid, Oumaïma Gharbi[*]*, Najet Sidi-Yakoub, Mai T.T. Tran, Mireille Turmine, Vincent Vivier*

Sorbonne Université, CNRS, Laboratoire Interfaces et Systèmes Électrochimiques (LISE), 4 place Jussieu F-75005 Paris, France

Sorbonne Université, CNRS, Laboratoire de Réactivité de Surface (LRS), 4 place Jussieu F-75005 Paris, France

[*]Corresponding author: E-mail address: oumaima.gharbi@sorbonne-universite.fr (O. Gharbi)

Highlights

- The addition of ammonium nitrate-based ionic liquids inhibited the anodic kinetics of an Al-Cu-Mg Al alloy, revealed by the presence of a large passivation plateau.
- The alkyl chain length slightly reduced the cathodic reaction, and the results suggested that the ammonium cation acted as a barrier to chloride ions.
- Selective dissolution of Cu-rich particles occurred when the ionic liquid was added to the NaCl solution.

Abstract

In this work, the effect of an ammonium nitrate ionic liquid on the corrosion susceptibility of an Al-Cu-Mg alloy was investigated. The effect of the nitrate anion and the ammonium cation on the anodic and cathodic kinetics were studied separately using potentiodynamic polarisation testing, electrochemical impedance spectroscopy and scanning electron

microscopy. The results revealed a significant anodic inhibition, associated with a cation/anion synergy. The cathodic kinetics however increase with the presence of nitrates, associated with nitrate reduction reaction. Conversely, longer alkyl chain seemed to reduce the effect of nitrates. Such findings are promising in the context of developing ecofriendly chromate alternatives.

Keywords: Corrosion inhibition, Ionic liquids, Al alloys, Electrochemical impedance spectroscopy

1 Introduction

Corrosion protection of structural alloys remains to this date a significant technological and economical challenge[1,2]. Besides the maintenance and repair costs, from an environmental aspect, most of the current coating technologies rely on toxic chemicals such as chromates[3–5]. In light of recent legislations (e.g., the Regulation Evaluation, Authorisation and Restriction of Chemicals - REACH), chromate use has been progressively banned from most coating formulations[6,7]. Nevertheless, several exemptions were granted, based on safety reasons, such as for Al alloys used in aerospace applications[3]. Since the early 1960s, numerous chromate replacement candidates have been explored including vanadium, rare earth elements, trivalent chromium, or lithium salts[8–14]. To date, lithium technology is one of the most promising candidates and is already commercialised broadly[15]. However, this technology relies on lithium ores, a highly prized resource, especially in the current context of energy transition, as lithium is the core component of most battery technologies[16].

In this context, new directions are to be explored and from a practical aspect, ionic liquids (ILs) appear as promising candidates for chromate salts replacement[17–21]. This class of salts is characterized by a melting temperature below 100 ℃, which makes them attractive for processing on a wide range of materials. In fact, one of the main benefits of this class of chemicals is their thermal, chemical/electrochemical stability, together with negligible vapour

pressure. From an industrial point of view, such properties can be beneficial in the context of primer technologies as ionic liquids can be readily integrated into epoxy or polyurethane coating as corrosion inhibitors, which necessitate curing at ~200 °C. Promising results have been reported in the literature by Forsyth et al., where phosphonium-based ionic liquids were used as conversion coatings for Mg alloys[17]. Several studies on steels were reported in the literature as well, in which the ionic liquids were studied as potential corrosion inhibitors and added at (mg/kg) levels in NaCl solutions[22–24]. The inhibitions mechanisms however remain rather unclear, probably due to the complexity of these electrolytes, as many parameters such as concentration, the chemical nature of anion and cation, and pH of solution will impact the mechanism.

Herein, the corrosion inhibition mechanism of a protic ionic liquid - butylammonium nitrate (BAN) - on an aluminium alloy AA2024-T6 is presented. Although the effect of BAN is not investigated as a pure solvent and is mixed with water, the physicochemical properties of the solutions used in this study are assimilated to concentrated saline solutions. For this reason, the term ionic liquid is used, as the synthesis of the inhibitors follows the ionic liquid synthesis path. In the future, these inhibitors are intended to be used as pure components to be introduced in a coating system.

In this work, potentiodynamic polarisation testing, electrochemical impedance spectroscopy (EIS) and scanning electron microscopy (SEM) characterisation were conducted on an Al-Cu-Mg based Al alloy (AA2024-T6) exposed to 0.1 mol/L NaCl in the presence butylammonium nitrate ionic liquid. The effects of the anion, the cation chain length as well as the ionic liquid concentration were investigated in order to picture the overall inhibition mechanism associated with this ionic liquid family. This study is intended to highlight the potential of this promising class of chemicals which potentially could be used as inhibitors for coating systems of tomorrow.

2 Experimental

2.1 Sample preparation

In this work, Al alloy sheets (2 mm thick) AA2024-T6 were used. The chemical composition is reported in Table 1. The alloy sheets were mounted in epoxy resin and ground mechanically using silica carbide paper with ethanol up to 4000 SiC finish. The exposed surface area was 0.7 cm^2.

2.2 Ionic liquid synthesis

The ionic liquid synthesis was performed by slow additions of concentrated nitric acid (68% in water) to butylamine (68% in water) and purchased from Sigma Aldrich, at a 1:1 molar ratio. The reaction was conducted in a temperature-controlled recirculating bath fixed at -10 ℃ by a cryothermostat to maintain the mixture temperature under 5 ℃ during the synthesis. BAN was subsequently lyophilised for water removal, and then characterised by density measurements and NMR analysis. Since these ILs are well known, these data were compared with the existing literature. Ethylammonium nitrate ionic liquid (EAN) and propylammonium nitrate (PAN) were synthesised and characterised following the same procedure.

2.3 Electrochemical measurements

All electrochemical measurements were performed using a multichannel Biologic potentiostat, an Ag/AgCl reference electrode ($E_{Ag/AgCl}$ = 0.199 V/ESH), and a Pt mesh as the counter electrode. Experiments were conducted in naturally aerated 0.1 mol/L NaCl solutions with controlled amount of BAN (1 wt.%, 5 wt.%, 10 wt.%, 30 wt.%, and 50 wt.%). It should be mentioned that for content above 50% in BAN, NaCl was no longer soluble in the mixture. The molar concentrations were determined and are reported in Table 2. The pH of the as-prepared solutions was measured prior to the experiments for all the solutions and was varying between 7.9 and 8.3. Electrochemical impedance spectroscopy analyses were systematically conducted for each measurement at the corrosion potential – or on the anodic

and cathodic branch ± 0.02 V vs. the corrosion potential (E_{corr}) when specified – after 10 h immersion at E_{corr}. The sinewave perturbation amplitude was fixed to 10 mV, peak to peak, between 2×10^{4}-10^{-3} Hz with 8 points per frequency decade. Potentiodynamic polarisation testings were performed following a 30 min immersion at OCP, started at E_{corr} -0.02 V vs. Ag/AgCl and stopped when the current reached 1 mA cm^{-2} for the anodic branch, whereas the cathodic branch was measured independently from E_{corr} + 0.02 V to -1.5 V vs. Ag/AgCl at a 1 mV s^{-1} scan rate. All solutions were prepared from reagent grade chemicals (NaCl and $NaNO_3$) purchased from Sigma Aldrich.

2.4 Microstructural characterisation

Surface topography and chemical composition were determined using ZEISS ULTRA 55 FEG SEM equipped with EDS (QUANTAX SDD), to understand the inhibition mechanism associated with the ionic liquids used in the study. Secondary and backscattered electron mode analysis was operated at 15 kV to identify corrosion products, localised attacks and sample surface composition after 24 h immersion in 0.1 mol/L NaCl, 0.1 mol/L NaCl + 10 wt.%, 30 wt.% and 50 wt.% BAN.

Table 1 Elemental composition (in wt.%) of the AA2024-T6 alloy used in this work.

Element	Al	Cu	Mg	Fe	Mn	Si	Ti	Cr	Zn	P	S	Ca
wt. %	Bal.	4.8	1.6	0.22	0.64	0.19	0.05	0.04	0.08	0.03	0.02	0.04

Table 2. Calculated molar concentration of the BAN mixtures used in this study.

% wt.	BAN 1%	BAN 5%	BAN 10%	BAN 30%	BAN 50%	BAN 100%

[BAN]	0.07	0.37	0.74	2.3	3.9	8.1

3 Results

3.1 Effect of BAN at different concentrations

3.1.1 Potentiodynamic polarisation testing of AA2024-T6 in the presence of BAN

In order to investigate the effect of BAN and depict a scenario reflecting a defect such as a scratch on a coating, various mass fractions of BAN with water (1 wt.%, 5 wt.%, 10 wt.%, 30 wt.%, and 50 wt.%) were investigated by potentiodynamic polarisation which is displayed in Fig. 1. Anodic behaviour was investigated separately (Fig. 1(a)) in order to visualize the impact of BAN concentration on the anodic kinetics (dissolution, passivation, pitting potential (E_{pit})) of the alloy. For reference, potentiodynamic polarisation measurements were also performed in a 0.1 mol/L NaCl solution, showing a sharp increase in the anodic current, with no distinction made between E_{corr} and E_{pit} indicating that stable pitting occurs at the vicinity of E_{corr}. Conversely, a slight shift of E_{pit} from E_{corr} is observed at low concentrations (1 wt.% and 5 wt.%) followed by an active domain. In fact, at 5% BAN, the active domain observed is also accompanied by the presence of a passive plateau ranging from 0.0 $V_{Ag/AgCl}$ to about 0.5 $V_{Ag/AgCl}$ suggesting the passivation of the AA2024-T6. Most importantly, however, is the significant decrease of about 3 orders of magnitude of the anodic current, which is observed for concentrations larger than 10 wt.% of BAN, and which is followed by an extended passive domain ranging from 0.3 $V_{Ag/AgCl}$ to 1.6 $V_{Ag/AgCl.}$ These results clearly indicate a significant inhibition of the anodic kinetics when BAN is introduced into solution, 10 wt.% BAN being the threshold concentration for a better inhibition.

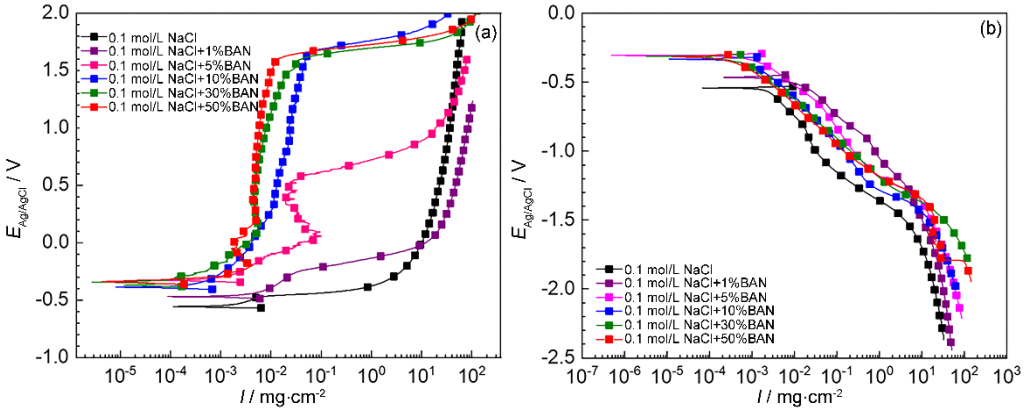

Fig. 1. (a) Representative anodic and (b) cathodic polarisation curves of AA2024-T6 in naturally aerated 0.1 mol/L NaCl (black) and in the presence of 1 wt.% (purple); 5 wt.% (pink); 10 wt.% (blue); 30 wt.% (green), and 50 wt.% (red) BAN.

Conversely, the cathodic polarisation curves displayed in Fig. 1(b) show an increase in the cathodic kinetics in the presence of BAN in solution. However, the addition of BAN at increasing concentrations did not change significantly the overall cathodic kinetics. The cathodic kinetics on AA2024-T6 is known to be dominated by the oxygen reduction reaction (ORR), but in this case, the result suggests that the mechanism involves the reduction of other species present at the solution-metal interface. At this stage, the main hypothesis related to the presence of this additional cathodic current is the reduction of nitrate anion (NO_3^-), known to reduce preferentially on Cu-rich sites[25–27]. The effect of NO_3^- anion on the anodic and cathodic kinetics will be discussed in further details in the next section.

3.1.2 Electrochemical impedance spectroscopy: influence of the ionic liquid concentration

Electrochemical impedance spectroscopy measurements were carried out after 10 h immersion in 0.1 mol/L NaCl and with the concentration of BAN as a parameter (Fig. 2). In 0.1 mol/L NaCl, the Nyquist representation reveals the presence of two time-constants, the first corresponding to a capacitive loop, followed by a ~40° slope. The characteristic

frequency of the first loop (1.1 Hz) is commonly associated with charge transfer resistance in parallel to the interfacial capacitance (probably dominated by the capacitance of the oxide layer as reported previously for pure aluminium [28]. The second time constant, however, might be attributed to a diffusion process of species inside a finite layer (which could be the outer porous layer which has a loose resistance to corrosion) known also as the finite-length Warburg impedance, as the value of the slope is close to 45° (the values measured graphically might be affected by an overlap of two loops which can slightly affect the actual value). Between 0.1 mol/L NaCl and 0.1 mol/L NaCl + 1 wt.% BAN, minimal changes are observed revealing a limited effect of the ionic liquid at such a concentration. It is only from 5 wt.% BAN in solution that a noticeable increase in the magnitude of the impedance response can be observed with the same overall shape, meaning probably that the corrosion mechanism is very similar.

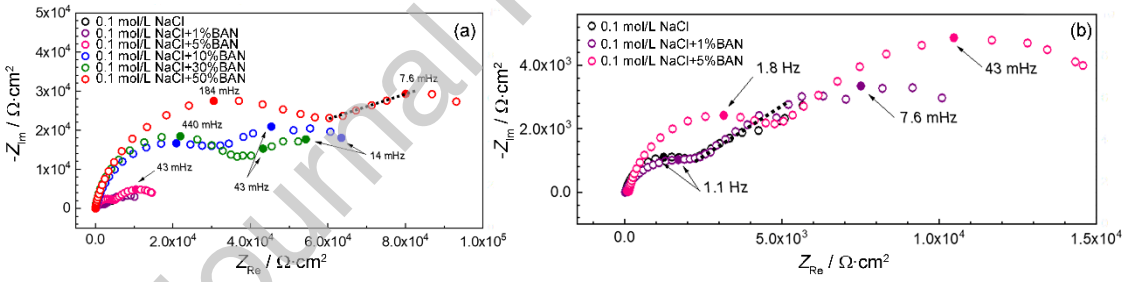

Fig. 2. Nyquist diagrams of the AA2024-T6 after 10 h immersion in 0.1 mol/L NaCl and 0.1 mol/L NaCl + 1 wt.%, 5 wt.%, 10 wt.%, 30 wt.%, 50 wt.% BAN (Fig. 2(b) is an enlarged version of Fig. 2(a) to show 0.1 mol/L NaCl and 1 wt.%, and 5 wt.% BAN).

The corrosion inhibition of AA2024-T6 by BAN becomes significant at a concentration larger than 10 wt.%, rationalising the results obtained by potentiodynamic polarisation testing. In fact, the impedance of the first loop increased by approximately one order of magnitude. This first capacitive loop is characterised by a time constant similar to what was reported in the

literature for the charge transfer resistance in parallel with the interfacial capacitance for Al dissolution. In this study, this first loop is influenced by BAN concentration (above 5 wt.%). Therefore, it can be hypothesised, that the addition of BAN at a concentration above 5 wt.% can slow down the charge transfer reaction - for instance by forming a thin protective film at the material surface. This film can cover or partially cover the surface, thus reducing the active surface area. Moreover, from the Nyquist representation, it is unclear at this stage whether the second loop is associated with a CPE or a diffusion mechanism. However, the low-frequency time constant shows a linear behaviour forming a 45° slope with the *x*-axis. This is usually a characteristic of a diffusion-limited process. The graphical analysis of the second loop as a function of BAN concentration revealed a decrease in the angle of the slope from ~40° to ~22° for concentrations larger than 10 wt.% BAN, indicating a change of the diffusion properties, typically reported in the literature to be associated with the diffusion inside pores[29]. The evolution of the slope angle as a function of BAN concentration is reported in Table 3.

Table 3. Parameters determined from EIS measurements performed in this study as a function of BAN concentration. α is the CPE parameter measured from the high-frequency capacitive-like loop, and θ corresponds to the angle of the diffusion low-frequency time constant.

Electrolyte	α	θ / **(°)**
0.1 mol/L NaCl	0.72	38.4
0.1 mol/L NaCl + 1 wt.% BAN	0.71	40.3
0.1 mol/L NaCl + 5 wt.% BAN	0.81	39.7
0.1 mol/L NaCl + 10 wt.% BAN	0.83	22.3
0.1 mol/L NaCl + 30 wt.% BAN	0.89	21.2

0.1 mol/L NaCl + 50 wt.% BAN	0.88	19.5

3.2 Effect of the cation chain length and nitrates on the anodic and cathodic kinetics

3.2.1 Potentiodynamic polarisation curves of AA2024-T6 in the presence of BAN, PAN, EAN and NO_3^-

Nitrates are known to be strong oxidants and their effect on Al has been largely documented in the literature. In order to solely investigate the effect of the NO_3^-, a $NaNO_3$ solution was prepared with a NO_3^- concentration equivalent to 10 wt.% BAN (0.7 mol/L) (Fig. 3). Conversely, the role of the cation was studied by varying the chain length of the alkyl chain at a fixed concentration (0.7 mol/L).

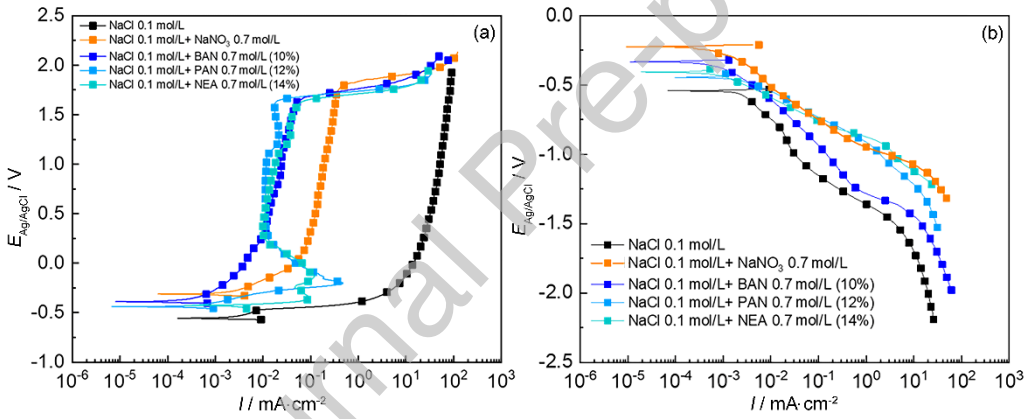

Fig. 3. Effect of the ammonium cation chain on the (a) anodic and (b) cathodic kinetics of the AA2024-T6.

The anodic polarisation curves reveal that in the presence of $NaNO_3$ in NaCl solution, at NO_3^- concentration equivalent to 10 wt.% BAN, the passive plateau is one order of magnitude higher than the results obtained with BAN, PAN and EAN. Such results highlight a probable cation-anion synergy on the inhibition mechanism. The passive plateau length, however, remains similar for the three ionic liquids, indicating a limited effect of the chain length on the anodic inhibition mechanism. Conversely, the cathodic polarisation curves show a very

different trend. In fact, as the chain length decreases, the cathodic slope, especially for the second part of the curve observed for potential lower than -0.8 V vs. Ag/AgCl, is very similar to the result obtained with $NaNO_3$, suggesting that nitrate reduction might be limited by the presence of long alkyl chains. In conclusion, the presence of the cation in solution further decreases the anodic current density plateau (by one order of magnitude), however the chain length does not induce change in the anodic kinetics (the passive current density). Contrastingly, the presence of shorter alkyl chain on the ammonium cation increases further the cathodic kinetics.

3.2.2 Electrochemical impedance spectroscopy: influence of chain length

Electrochemical impedance spectroscopy measurements were performed on the AA2024-T6 in presence of BAN, PAN, EAN and NO_3^- (Fig. 4). In the presence of NO_3^-, only a single capacitive loop can be seen, associated with the charge transfer process and is much larger than in NaCl solution, thus corroborating the hypothesis of an Al passivation by NO_3^- (discussed in the next section). In this case, however, the second loop was not seen on the low-frequency part of the spectra, but the very low-frequency part has been truncated to avoid the non-stationarity effect of the system on long time. A similar observation can be made with the EAN. However, as the cation chain length increases such as for PAN and BAN, with the presence of the characteristic second loop with a 22.5° slope, as discussed previously. Interestingly, the second loop becomes better defined as the ammonium cation chain length increases. The characteristic frequency of the second loop is for BAN 10 wt.% at about 14 mHz, which, together with the decrease in slope at 22°, suggests that the diffusion process might be occurring in pores. At this stage, the results suggest that the presence of the second loop is mostly associated with the ammonium cation and its chain length plays a role in the inhibition mechanism.

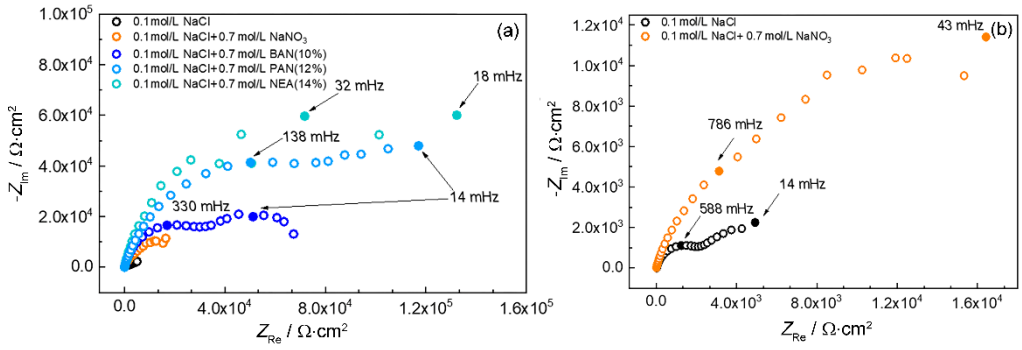

Fig. 4. Electrochemical impedance results in Nyquist representation of the AA2024-T6 after 10 h exposure in 0.1 mol/L NaCl, 0.1 mol/L NaCl + 0.7 mol/L BAN/PAN/EAN and 0.1 mol/L NaCl + 0.7 mol/L $NaNO_3$ (Fig. 4(b) is an enlarged version of Fig. 4(a) to show 0.1 mol/L NaCl and 0.1 mol/L NaCl + 0.7 mol/L $NaNO_3$).

3.3 Microstructural characterisation of AA2024-T6 before and after BAN exposure

The effect of BAN on the surface and particularly on the localised corrosion process was investigated using SEM. The surface topography and chemical contrast (secondary electrons and backscattered electrons modes) of the AA2024-T6 surface before (Fig. 5 (a0)) and after 24 h immersion in 0.1 mol/L NaCl (Fig. 5 (a1) and (a2)), 0.1 mol/L NaCl + 10 wt.% BAN (Fig. 5(b1) and (b2)), 0.1 mol/L NaCl + 30 wt.% BAN (Fig. 5(c1) and (c2)) and 0.1 mol/L NaCl + 50 wt.% BAN (Fig. 5(d1) and (d2)) were investigated. The AA2024-T6 surface before testing shows the presence of large intermetallic particles with sizes ranging from several micrometer to ~15-20 µm. EDX analysis revealed the presence of Cu-rich particles, as expected for this alloy family, and particularly the presence of the S-phase (Al_2CuMg) the Al_7Cu_2Fe phase and the θ-phase (Al_2Cu). After 24 h exposure in 0.1 mol/L NaCl clearly shows signs of extensive localised corrosion. The presence of small and large pits throughout the matrix, corrosion products around the large pits, and trenches surrounding intermetallic particles, reveals important pitting and trenching caused by the difference in the

electrochemical potential between the particles and the matrix. Conversely, after BAN addition, the alloy does not reveal any sign of significant pitting or corrosion product accumulation on the matrix. Interestingly, only a few areas were attacked, indicating a selective dissolution of several intermetallic particles. Such observation, however, does not provide more information on the dissolution mechanism involved (*i.e.*, chemical or electrochemical process). Overall, the microstructural observations emphasise the presence of two areas with distinct surface reactivities, with the passive Al matrix and large active cavities that could be assimilated to pores. The SEM observations, however, do not reveal the formation of a protective film. More detailed surface analysis such as XPS should be realised in future work.

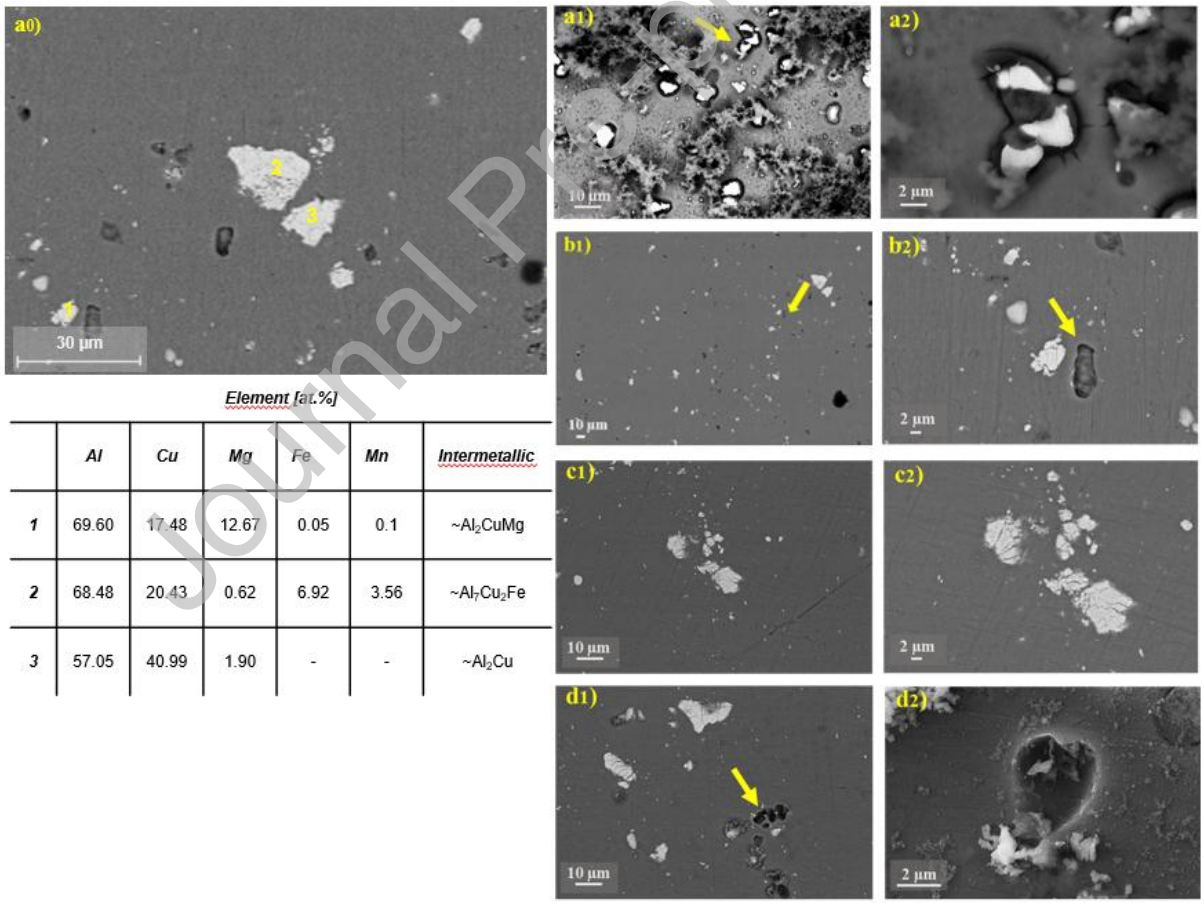

Element [at.%]

	Al	*Cu*	*Mg*	*Fe*	*Mn*	*Intermetallic*
1	69.60	17.48	12.67	0.05	0.1	~Al_2CuMg
2	68.48	20.43	0.62	6.92	3.56	~Al_7Cu_2Fe
3	57.05	40.99	1.90	-	-	~Al_2Cu

Fig. 5. SEM micrographs in BSE (a1, b1, c1, d1) and enlarged areas in SE (a2, b2, c2, d2) mode of the AA2024-T6 surface before exposure (a0), after 24 h immersion in (a1, a2) 0.1

mol/L NaCl exposure, (b1, b2) 0.1 mol/L NaCl+10 wt.% BAN, (c1, c2) 0.1 mol/L NaCl+30 wt.% BAN and (d1, d2) 0.1 mol/L NaCl+50 wt.% BAN.

4 Discussion

The corrosion mechanism of Al alloys is known to be highly dependent on the microstructure[30–32]. More specifically, the intermetallic particle population, distribution and size, provide preferential sites for corrosion initiation. In this work, an AA2024-T6 was exposed to 0.1 mol/L NaCl solution with and without the presence of ammonium nitrates ionic liquids. Besides the heterogeneous nature of Al-Cu-Mg alloys[33,34], chloride containing electrolytes are also known to be highly aggressive towards Al alloys, causing pitting and passivity breakdown[35–37]. In this section, and based on the experimental evidence and the literature, an overall mechanism which includes the corrosion initiation process induced by chlorides as well as the inhibition mechanism will be discussed and is presented in Fig. 6. On Al matrix, and with the Cl^- species in solution, the pitting initiation mechanism occurs through the following steps: i) Cl^- adsorption on the oxide film caused by a chemical reaction between Cl^- and the film, leading to the oxide thinning, ii) Al-chloride species formation, and finally, iii) exposure of the bare Al surface[30,38,39]. In the presence of NO_3^-, however, the dissolution mechanism is inhibited, as NO_3^- are known to be strong oxidants, yielding to iii) NO_3^- reduction on bare Al metal[27,40]. In fact, this was corroborated by the passivation plateau seen on the potentiodynamic polarisation results and the microstructural observations, revealing the absence of corrosion products and pitting on the Al matrix. The ability of NO_3^- anions to be reduced by metallic Al (after being exposed) has been documented previously through the following mechanism[27,41], involving Al^{3+} cation from $Al_2O_3.nH_2O$:

$$Al^{3+} + 2Cl^- + 2H_2O \rightarrow Al(OH)_2Cl_2^- + 2H^+ \quad (1)$$

$$Al \rightarrow Al^{3+} + 3e^{-} \quad (2)$$

$$Al^{3+} + 4Cl^{-} \rightarrow AlCl_4^{-} \quad (3)$$

$$AlCl_4^{-} + 2H_2O \rightarrow Al(OH)_2Cl + 2H^{+} + 3Cl^{-} \quad (4)$$

$$3NO_3^{-} + 8Al + 18H_2O \rightarrow 3NH_3 + 8Al(OH)_3 + 3OH^{-} \quad (5)$$

However, the Al passivation can be partially explained by the presence of nitrates in the ionic liquids as the results also highlighted the role of the ammonium cation on the passivation mechanism. In fact, it was seen on Fig. 3(a) that for similar NO_3^- concentrations, the passivation plateau in the presence BAN (butylammonium + nitrates) was one order of magnitude lower than the results shown for NO_3^-. Such observations reveal a synergistic effect between the anion and the cation chain, further reducing the anodic current density plateau. In fact, the synergistic effect of several anions and a tetra-n-butylammonium cation has been investigated previously by Aramaki et al. in the context of Fe corrosion in acid solution[42,43]. It was reported that the addition of the tetra-n-butylammonium cation yielded to an increase of the anion surface coverage and a stabilisation by electrostatic interactions. Nonetheless, the electrochemical and surface characterisation did not provide a clear idea on the nature of the cation-substrate interaction. Another hypothesis of this work emitted in this work is the blocking effect of the ammonium species on the surface from aggressive chloride ions penetration.

On the intermetallic particles, however, such as Al_2Cu and Al_7Cu_2Fe, the electrochemical reactions involve a multistep process. As revealed by the potentiodynamic polarisation tests, NO_3^- addition resulted in a cathodic current density increase characterised by two distinct slopes. At the open circuit potential, the reduction mechanism could be separated into two stages: the first stage involves the i) oxygen reduction reaction (ORR) known to occur on the intermetallic particles (*i.e.*, Cu-rich particles), as ORR progresses, O_2 depletion is accelerated

at the electrolyte-surface interface and yields to a second stage involving ii) nitrate reduction to nitrites with the concomitant Cu oxidation, known to be preferentially oxidised by NO_3^- species. After a certain incubation period, a second reduction reaction - also highlighted by the dramatic current density increase from *E*= -0.8 V vs. Ag/AgCl - albeit nitrites reduction is initiated through the following reactions as reported by Foley et al. involving Cu from intermetallic particles[27]:

$$O_2 + 2H_2O + 4e^- \rightarrow 4OH^- \quad (6)$$

$$NO_3^- + 2e^- + H_2O \rightarrow NO_2^- + 2OH^- \quad (7)$$

$$Cu \rightarrow Cu^{2+} + 2e^- \quad (8)$$

$$NO_2^- + 6e^- + 5H_2O \rightarrow NH_3 + 7OH^- \quad (9)$$

With the presence of NH_3 in solution, the chemical dissolution of the Cu present on the intermetallic yields to the formation of the large pits - corroborated by the SEM observations after 24 h immersion - through the following reaction:

$$Cu^{2+} + 4NH_3 \rightarrow Cu(NH_3)_4^{2+} \quad (10)$$

The formation of large pits might explain the low frequency diffusional loop observed on the Nyquist spectra on Figs. 2 and 4. The characteristic frequency of the second time-constant (~14 mHz) seems too low to be attributed to a surface-electrolyte diffusion process, which was found to be around 250 mHz, as reported by Keddam et al. in a study of Al alloy AA2219-T87 exfoliation corrosion mechanism in an EXCO solution[44]. Moreover, such a surface-electrolyte diffusion process will not be sensitive to minute change in the porosity of the interface. In this work, the impact of the viscosity of the mixtures on the diffusional processes was considered to not vary significantly as reported previously by Xu who measured the viscosity of n-butylammonium nitrate mixtures [45]. In this scenario, the

presence of alkylammonium cation in the electrolyte may also play a role in the cathodic reactions and adsorb on the surface such as the cathodic sites. The alkylammonium adsorption will be in competition with O_2 and NO_3^- reduction. Under these specific conditions, the EAN, PAN and BAN and $NaNO_3$ mixtures were prepared in order to obtain similar NO_3^- anion available, in fact, NO_3^- anions are known to be weak complexing agents, rather favouring complete dissociation, as reported for BAN ionic liquid in the work of Bou Malham et al [46]. In fact, this hypothesis can explain the cathodic polarisation results, revealing that an increase in the cation chain length was limiting the dramatic current density increase caused by NO_3^- and NO_2^- reduction, particularly on the lower cathodic potential (E < -0.8 $V_{Ag/AgCl}$). Similar observations were made by Zhang et al. who investigated the effect of quaternary ammonium-based ionic liquid on the electrodeposition mechanism of Cu[47]. The addition of an ammonium-based ionic liquid in the solution resulted in a decrease in the cathodic peak current density related to Cu reduction, explained by strong adsorption of the quaternary ammonium cation on the cathodic sites, competing with Cu reduction reaction. Their results also revealed a greater surface absorbability of the quaternary ammonium cation with longer alkyl chains. Such a hypothesis also rationalises the idea of a chain length effect (*i.e.*, longer alkyl chains will more efficiently block cathodic sites for NO_3^- reduction reactions) and can explain such differences between the NO_3^-, EAN, PAN and BAN cathodic polarisation tests as seen in Figs. 3 and 4.

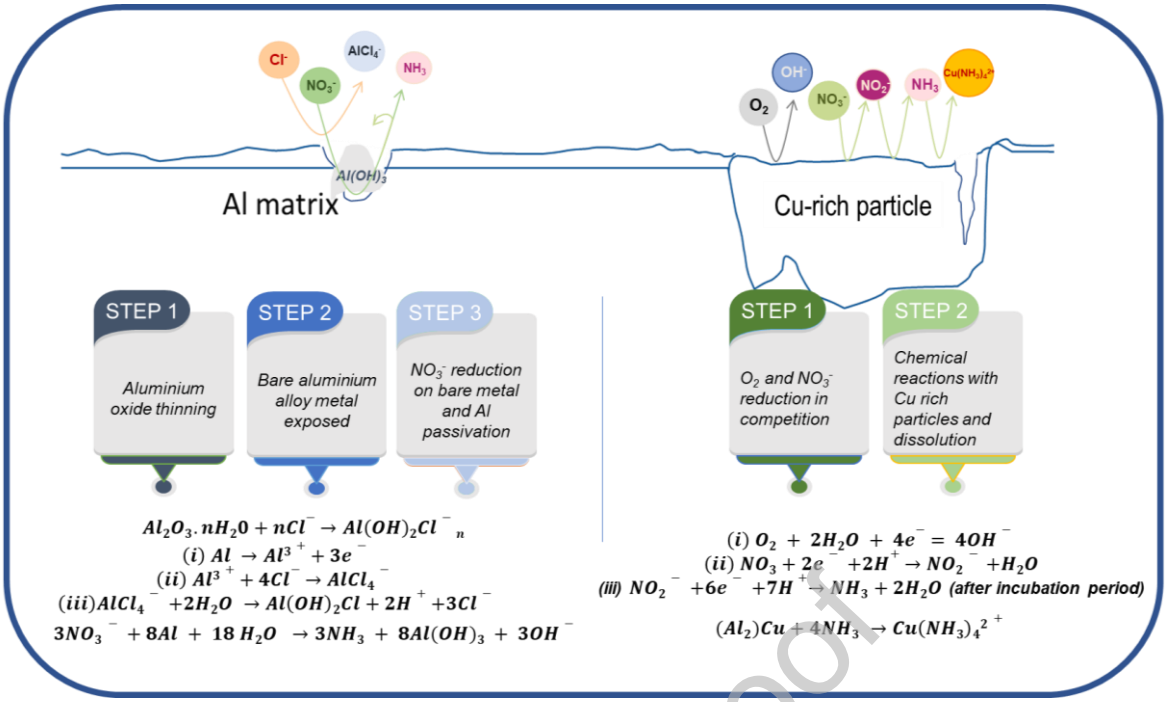

Fig. 6. Schematic figure illustrating the overall mechanism of this work. On the Al matrix, Al dissolution and passivation occur, promoted by the presence of Cl^- and NO_3^- species. On the Cu-rich particles, O_2 reduction and nitrate reduction are the primary reactions followed by nitrite reduction and Cu dissolution.

5 Conclusion

In this work, three ammonium-based ionic liquids were used as potential corrosion inhibitors for an AA2024-T6 Al alloy. Herein, the ionic liquid concentration and the effect of the chain length on the anodic and cathodic kinetics were investigated by electrochemical impedance spectroscopy, potentiodynamic polarisation testing and SEM characterisation. After 24 h immersion tests, the Al alloy surface was significantly less attacked, with the presence of preferential dissolution at the intermetallic particles. The anodic polarisation testing and the electrochemical impedance spectroscopy results revealed inhibition of the anodic kinetics, as seen by the presence of a passivation plateau and the increase of the first capacitive loop associated with the charge transfer reaction. Interestingly, the chain length seemed to not significantly affect the anodic kinetics but rather the cathodic reaction mechanism as reported

by the cathodic polarisation testing. In fact, the cathodic polarisation curves indicate that increasing the chain length (passing from BAN to EAN) limits the cathodic reaction, which is, according to the literature, due to ammonium cation adsorption, limiting available site for NO_3^- reduction. From the experimental observations and according to the literature, a three stages mechanism is proposed as shown in Fig. 6, which will be further investigated in the future:

- The anodic reaction is dominated by Al dissolution and passivation, promoted by the presence of nitrates in solution.
- The cathodic reaction can be described by (i) O_2 reduction, which is followed by (ii) NO_3^- reduction once O_2 depletion occurs.
- Nitrite reduction to NH_3 induces Cu-rich particles dissolution, leading to the formation of large "pores" on the Al alloy surface.

Acknowledgments

Abdelmoheiman Zakaria Benbouzid acknowledges Ecole Militaire Polytechnique d'Alger, Algeria for his PhD grant.

The authors would like to thank Stephanie Delbrel for the SEM analysis.

Declaration of Competing Interest

The authors declare that they have no known competing financial interests or personal relationships that could have appeared to influence the work reported in this paper.

References

[1] B. Hou, X. Li, X. Ma, C. Du, D. Zhang, M. Zheng, W. Xu, D. Lu, F. Ma, The cost of corrosion in China, npj Mater. Degrad. 1 (2017) 4.

[2] N.G. Thompson, M. Yunovich, D. Dunmire, Cost of corrosion and corrosion

maintenance strategies, Corros. Rev. 25 (2007) 247–262.

[3] O. Gharbi, S. Thomas, C. Smith, N. Birbilis, Chromate replacement: what does the future hold? npj Mater. Degrad. 2 (2018) 12.

[4] J. Sinko, Challenges of chromate inhibitor pigments replacement in organic coatings, Prog. Org. Coat. 42 (2001) 267–282.

[5] R.L. Twite, G.P. Bierwagen, Review of alternatives to chromate for corrosion protection of aluminum aerospace alloys, Prog. Org. Coat. 33 (1998) 91–100.

[6] The European Parliament And The Council, Regulation (EC) No 1907/2006 of the European parliament and of the council of 18 December 2006 concerning the Registration, Evaluation, Authorisation and Restriction of Chemicals (REACH), establishing a European Chemicals Agency, amending Directive 199, 2006.

[7] European Commission, Commission Regulation (EU) No 143/2011 of 17 February 2011 amending Annex XIV to Regulation (EC) No 1907/2006 of the European Parliament and of the Council on the Registration, Evaluation, Authorisation and Restriction of Chemicals ('REACH'), Off. J. Eur. Union. (2014) L244/6-L244/9.

[8] H. Guan, R.G. Buchheit, Corrosion protection of aluminum alloy 2024-T3 by vanadate conversion coatings, Corrosion 60 (2004) 284–296.

[9] A.E. Hughes, J.D. Gorman, P.R. Miller, B.A. Sexton, P.J.K. Paterson, R.J. Taylor, Development of cerium-based conversion coatings on 2024-T3 Al alloy after rare-earth desmutting, Surf. Interface Anal. 36 (2004) 290–303.

[10] B.W. Whitman, L. Li, G.M. Swain, Anti-corrosion properties of a TCP pretreatment conversion coating on aluminum alloy 2024-T3 during moist SO_2 atmospheric testing: Effects of galvanic coupling, J. Electrochem. Soc. 164 (2017) 135–147.

[11] J. Qi, Trivalent Chromium Conversion Coatings on Al and Al-Cu alloys, Ph. D. Thesis, University of Manchester, 2015.

[12] J.A. Bishopp, D. Jobling, G.E. Thompson, The surface pretreatment of aluminium-lithium alloys for structural bonding, Int. J. Adhes. Adhes 10 (1990) 153–160.

[13] P. Visser, Y. Liu, H. Terryn, J.M.C. Mol, Lithium salts as leachable corrosion inhibitors and potential replacement for hexavalent chromium in organic coatings for the protection of aluminum alloys, J. Coat. Technol. Res. 13 (2016) 557–566.

[14] A. Hughes, J. Laird, C. Ryan, P. Visser, H. Terryn, A. Mol, Particle characterisation and depletion of Li_2CO_3 inhibitor in a polyurethane coating, Coatings 7 (2017) 106.

[15] A. Kosari, F. Tichelaar, P. Visser, H. Zandbergen, H. Terryn, J.M.C. Mol, Laterally-resolved formation mechanism of a lithium-based conversion layer at the matrix and intermetallic particles in aerospace aluminium alloys, Corros. Sci. 190 (2021) 109651.

[16] F. Meng, J. McNeice, S.S. Zadeh, A. Ghahreman, Review of lithium production and recovery from minerals, brines, and lithium-ion batteries, Miner. Process. Extr. Metall. Rev. 42 (2021) 123–141.

[17] J. Sun, P.C. Howlett, D.R. MacFarlane, J. Lin, M. Forsyth, Synthesis and physical property characterisation of phosphonium ionic liquids based on $P(O)_2(OR)_2^-$ and $P(O)_2(R)_2^-$ anions with potential application for corrosion mitigation of magnesium alloys, Electrochim. Acta 54 (2008) 254–260.

[18] H.H. Elsentriecy, J. Qu, H. Luo, H.M. Meyer, C. Ma, M. Chi, Improving corrosion resistance of AZ31B magnesium alloy via a conversion coating produced by a protic ammonium-phosphate ionic liquid, Thin Solid Films 568 (2014) 44–51.

[19] H.H. Elsentriecy, H. Luo, H.M. Meyer, L.L. Grado, J. Qu, Effects of pretreatment and process temperature of a conversion coating produced by an aprotic ammonium-phosphate ionic liquid on magnesium corrosion protection, Electrochim. Acta 123 (2014) 58–65.

[20] P.C. Howlett, S. Gramet, J. Lin, J. Efthimiadis, X.B. Chen, N. Birbilis, M. Forsyth,

Conversion coatings of Mg-alloy AZ91D using trihexyl(tetradecyl) phosphonium bis(trifluoromethanesulfonyl)amide ionic liquid, Sci. China Chem. 55 (2012) 1598–1607.

[21] M. Forsyth, P.C. Howlett, S.K. Tan, D.R. MacFarlane, N. Birbilis, An ionic liquid surface treatment for corrosion protection of magnesium alloy AZ31, Electrochem. Solid-State Lett. 9 (2006) 52–55.

[22] C. Verma, E.E. Ebenso, M.A. Quraishi, Ionic liquids as green and sustainable corrosion inhibitors for metals and alloys: An overview, J. Mol. Liq. 233 (2017) 403–414.

[23] N. V. Likhanova, M.A. Domínguez-Aguilar, O. Olivares-Xometl, N. Nava-Entzana, E. Arce, H. Dorantes, The effect of ionic liquids with imidazolium and pyridinium cations on the corrosion inhibition of mild steel in acidic environment, Corros. Sci. 52 (2010) 2088–2097.

[24] D. Guzmán-Lucero, O. Olivares-Xometl, R. Martínez-Palou, N.V. Likhanova, M.A. Domínguez-Aguilar, V. Garibay-Febles, Synthesis of selected vinylimidazolium ionic liquids and their effectiveness as corrosion inhibitors for carbon steel in aqueous sulfuric acid, Ind. Eng. Chem. Res. 50 (2011) 7129–7140.

[25] E. Pérez-Gallent, M.C. Figueiredo, I. Katsounaros, M.T.M. Koper, Electrocatalytic reduction of Nitrate on Copper single crystals in acidic and alkaline solutions., Electrochim. Acta 227 (2017) 77–84.

[26] M. Hou, Y. Tang, J. Xu, Y. Pu, A. Lin, L. Zhang, J. Xiong, X.J. Yang, P. Wan, Nitrate reduction in water by aluminum-iron alloy particles catalyzed by copper, J. Environ. Chem. Eng. 3 (2015) 2401–2407.

[27] A. Adams, K. Eagle, T. Foley, Synergistic effects of anions in the corrosion of aluminum, ECS Electrochem. Lett. 119 (1967) 1692–1694.

[28] T.T.M. Tran, B. Tribollet, E.M.M. Sutter, New insights into the cathodic dissolution of

aluminium using electrochemical methods, Electrochim. Acta 216 (2016) 58–67.

[29] O.E. Barcia, E. D'Elia, I. Frateur, O.R. Mattos, N. Pébère, B. Tribollet, Application of the impedance model of de Levie for the characterization of porous electrodes, Electrochim. Acta 47 (2002) 2109–2116.

[30] R.T. Foley, Localized corrosion of aluminum alloys—A review, Corrosion 42 (1986) 277–288.

[31] N. Birbilis, Y.M. Zhu, S.K. Kairy, M.A. Glenn, J.F. Nie, A.J. Morton, Y. Gonzalez-Garcia, H. Terryn, J.M.C. Mol, A.E. Hughes, A closer look at constituent induced localised corrosion in Al-Cu-Mg alloys, Corros. Sci. 113 (2016) 160–171.

[32] G.M. Scamans, N. Birbilis, R.G. Buchheit, Corrosion of aluminum and its alloys, in: T. Richardson, B. Cottis, R. Lindsay, S. Lyon, D. Scantlebury, H. Stott, M. Graham eds., Shreir's Corrosion, Elsevier, Amsterdam, 2010, pp. 1975–2008.

[33] T.H. Muster, A.E. Hughes, G.E. Thompson, Copper Distributions in Aluminium Alloys, Nova Science Publishers Inc., New York, 2009.

[34] I. Polmear, D. StJohn, N. Jian-Feng, Q. Ma, Light Alloys : Metallurgy of the Light Metals, Fifth Edit, Elsevier, Amsterdam, 2017.

[35] V. Guillaumin, G. Mankowski, Localized corrosion of 2024 T351 aluminium alloy in chloride media, Corros. Sci. 41 (1999) 421–438.

[36] N. Murer, R.G. Buchheit, Stochastic modeling of pitting corrosion in aluminum alloys, Corros. Sci. 69 (2013) 139–148.

[37] G.S. Chen, M. Gao, R.P. Wei, Microconstituent-induced pitting corrosion in aluminum alloy 2024-T3, Corros. Sci. 52 (1996) 8–15.

[38] T.H. Nguyen, R.T. Foley, The chemical nature of aluminum corrosion: III . the dissolution mechanism of aluminum oxide and aluminum powder in various electrolytes, J. Electrochem. Soc. 127 (1980) 2563–2566.

[39] G.S. Frankel, Pitting Corrosion, in: S.D.C. and B.S. Covino (Ed.), Met. Handb., ASM International, 2003, pp. 1–6.

[40] G.T. Burstein, R.M. Organ, Repassivation and pitting of freshly generated aluminium surfaces in acidic nitrate solution, Corros. Sci. 47 (2005) 2932–2955.

[41] N.B. Milic, Z.D. Bugarcic, P.T. Djurdjevic, Hydrolysis of aluminum(III) ion in sodium nitrate medium, Can. J. Chem. 69 (1991) 28–32.

[42] K. Aramaki, M. Hagiwara, H. Nishihara, The synergistic effect of anions and the ammonium cation on the inhibition of iron corrosion in acid solution, Corros. Sci. 27 (1987) 487–497.

[43] C. Pan, X. Wang, Y. Behnamian, Z. Wu, Z. Qin, D.-H. Xia, W. Hu, Monododecyl phosphate film on LY12 aluminum alloy: pH-controlled self-assembly and corrosion resistance, J. Electrochem. Soc. 167 (2020) 161510.

[44] M. Keddam, C. Kuntz, H. Takenouti, D. Schuster, D. Zuili, Exfoliation corrosion of aluminium alloys examined by electrode impedance, Electrochim. Acta 42 (1997) 87–97.

[45] Y. Xu, B. Chen, W. Qian, H. Li, Properties of pure n-butylammonium nitrate ionic liquid and its binary mixtures of with alcohols at T = (293.15 to 313.15) K, J. Chem. Thermodyn. 58 (2013) 449–459.

[46] I. Bou Malham, P. Letellier, A. Mayaffre, M. Turmine, Part I: Thermodynamic analysis of volumetric properties of concentrated aqueous solutions of 1-butyl-3-methylimidazolium tetrafluoroborate, 1-butyl-2,3-dimethylimidazolium tetrafluoroborate, and ethylammonium nitrate based on pseudo-lattice theory, J. Chem. Thermodyn. 39 (2007) 1132–1143.

[47] Q. Zhang, X. Yu, Y. Hua, W. Xue, The effect of quaternary ammonium-based ionic liquids on copper electrodeposition from acidic sulfate electrolyte, J. Appl. Electrochem. 45 (2015) 79–86.